

SEVENTEENTH EUROPEAN ROTORCRAFT FORUM

Paper No. 91 -77

RESEARCH ON MEASUREMENT AND CONTROL OF
HELICOPTER ROTOR RESPONSE

USING BLADE-MOUNTED ACCELEROMETERS

1990 - 91

NORMAN D. HAM
M.I.T.
CAMBRIDGE, MA, U.S.A.

ROBERT M. MCKILLIP JR.
PRINCETON UNIVERSITY
PRINCETON, NJ, U.S.A.

SEPTEMBER 24 - 26, 1991
Berlin, Germany

Deutsche Gesellschaft für Luft- und Raumfahrt e.V. (DGLR)
Godesberger Allee 70, 5300 Bonn 2, Germany

OPGENOMEN IN
GEAUTOMATISEERDE
CIT. LOGUS

Nb1346



10/10/10

**RESEARCH ON MEASUREMENT AND CONTROL OF HELICOPTER ROTOR
RESPONSE USING BLADE-MOUNTED ACCELEROMETERS 1990-91**

Norman D. Ham
M.I.T.

Robert M. McKillip Jr.
Princeton University

ABSTRACT

Preliminary wind tunnel tests of the full-size Model 412/IBC rotor at the Ames Research Center, NASA, are described.

Blade lag motion was excited by swash plate oscillation, and the lag response was measured using blade-mounted accelerometers and compared with measurements using a conventional angle transducer.

The recorded open-loop accelerometer signals were used as input to the lag-IBC system in the laboratory. The resulting controller cyclic pitch outputs are compared with the original cyclic pitch excitation inputs, and the potential effectiveness of the controller in suppressing the original excitation is evaluated.

Recent developments in IBC technology and related rotor state measurements are briefly described in an appendix.

The test disturbance was sinusoidal longitudinal (or lateral) displacement of the cyclic controls. This technique has been used successfully in the past⁴. As shown in Reference 1, the closed-loop damping of blade lag motion is augmented by feeding back the lag rate to blade pitch.

Lag excitation tests were run at advance ratios 0 and .10 using swash plate excitation frequencies ω given by $\Omega - \omega = 0.9 \omega_L$ to $1.10 \omega_L$. A typical lag response time history and frequency spectrum from the tests is shown in Figs. 3 and 4. The swash plate excitation frequency ω appears in the rotating systems as $(\Omega \pm \omega)$ where Ω is the rotor frequency. At lag resonance $\Omega - \omega = \omega_L$.

The paper presents comparisons of measured and estimated lag displacements for the above test conditions, using the techniques of Ref. 2. In addition, the controller cyclic pitch outputs of Fig. 2 are compared with the original cyclic pitch excitation inputs, and the potential effectiveness of the controller in suppressing the original excitation is evaluated.

1. INTRODUCTION

Next-generation high-agility and low-vibration helicopters will require the measurement and control of rotor blade flapping, lagging, and bending. Theoretical and experimental research described in References 1, 2, and 3 has shown that blade-mounted accelerometers can be used as sensors for control of the blades individually or by swash plate.

Through other means of measuring flapping, lagging, and bending states are available, accelerometers permit the avoidance of conventional angle transducers and strain gauges, which are unreliable and difficult to mount, particularly on elastomeric-hinged or hingeless blades. In addition, accelerometers offer the capability of obtaining flapping and bending rates by integration of blade acceleration,^{1,2} rather than by estimation techniques involving either accurate knowledge of process dynamics or simplifying assumptions ignoring such dynamics.

Wind tunnel testing of the Model 412 rotor (Fig. 1) produced measurements of blade lag motion in inertial space for all four blades, using blade-root-mounted accelerometers. In the IBC system, Figure 2, these measurements are used to determine blade in-plane acceleration, estimated velocity, and displacement signals for each blade, and these signals are combined to generate inputs to the swash plate actuators; in the closed-loop system these inputs would provide helicopter blade in-plane damping augmentation.

Initial tests were open-loop, i.e., the output of the IBC system was not connected to the swash plate actuators. However, considerable insight into the closed-loop performance of the IBC system was obtained from the open-loop testing, as described below.

Recorded open-loop accelerometer signals were used as input to the IBC system of Figure 2 in the laboratory. The resulting cyclic control outputs were then compared with the desired closed-loop control displacements under the same disturbed test conditions.

This research was sponsored by the Ames Research Center, NASA, under Cooperative Agreement NCC-2-366.

2. THEORETICAL DISCUSSION

The lag acceleration at any spanwise station of the blade can be shown to be:

$$\frac{a_L}{R\Omega^2} = (x - \xi) \ddot{\zeta} + \xi \zeta$$

where R = rotor radius
 Ω = rotor rotational speed
 x = blade spanwise station r/R
 ξ = lag hinge spanwise station e_L/R
 ζ = blade lag angle

It is evident that if lag-oriented accelerometers are located at two spanwise stations, e.g. at x_1 and x_2 , subtraction of the two accelerometer signals will yield, from equation (1), the lag acceleration, i.e.,

$$\frac{a_{L2}}{R\Omega^2} - \frac{a_{L1}}{R\Omega^2} = (x_2 - x_1) \ddot{\zeta} \quad (2)$$

or alternatively, the lag displacement, i.e.,

$$(x_2 - \xi) \frac{a_{L2}}{R\Omega^2} - (x_1 - \xi) \frac{a_{L1}}{R\Omega^2} = \xi (x_2 - x_1) \zeta \quad (3)$$

Then the McKillip filter can be used to obtain lag rate $\dot{\zeta}$.

Experimental verification of lag damping augmentation can be obtained by oscillating the swash plate at frequency ω . The resulting blade pitch time history is

$$\theta_1 = \bar{\theta}_1 \sin \Omega t \sin \omega t + \frac{1}{2} \bar{\theta}_1 \cos(\Omega - \omega)t - \frac{1}{2} \bar{\theta}_1 \cos(\Omega + \omega)t$$

Then when $(\Omega - \omega) \rightarrow \omega_L$ the lag mode will be excited.

3. DESCRIPTION OF TEST EQUIPMENT

The following technical description is quoted verbatim from Ref. 5:

"The model 412 rotor system is a flexbeam design, with flapping freedom provided by primary and secondary flapping flexures machined in the yokes. The primary flexure is a tension beam tapered in thickness and width to maintain a constant stress. The secondary flapping flexure utilizes the distance between the pitch change bearings to provide additional flapping freedom.

"The elastomeric elements accommodate pitch-change and lead-lag motion, and also react blade beam and chord moments and centrifugal force. The outboard elastomeric bearing has conical and spherical elements, as shown in Figure 1. The lead-lag hinge is defined by the focal point of the spherical elements and the conical section is used to increase the radial stiffness of the bearing. The blade centrifugal force and torsional motion is carried through both the conical and spherical sections of the outboard bearing. The lead-lag motion is accommodated by the spherical motion.

"The damper bearing (inboard bearing) has radial and spherical elastomeric elements. This bearing is bonded to the spindle and transmits blade lead-lag motion to the damper that is attached to the bearing outer member.

The following technical description was provided by Ruth M. Heffernan, Ames Research Center, NASA:

"The 412 rotor system was tested in the NASA Ames 40- by 80- Foot Wind Tunnel. The rotor was instrumented to measure blade accelerations in two locations on each of the four blades, as well as the collective pitch, flapping angle, and lead-lag angle of the blades. For the IBC portion of the test, the rotor was excited through the swashplate at specific frequencies, and the uncontrolled blade response was recorded.

"Two miniature Entran accelerometers were mounted near the root of each rotor blade (eight accelerometers total). On each blade, the accelerometers were located at radial stations $.054r/R$ and $.069 r/R$. Each accelerometer was mounted on a split ring which fit around the blade spindle. The accelerometers can be oriented to measure either blade flapping or lead-lag acceleration. The blade accelerometer locations are shown in the rotor hub schematic shown in Fig. 1.

"Blade pitch was measured with a rotary potentiometer. The potentiometer, which was attached rigidly to the hub, was connected to the blade via a gear. In this way, torsional motion of the blade was recorded as a change in electric potential. The rotary potentiometer was located near the pitch bearing.

"Since this was a hingeless rotor, there were no hinges at which to measure either the flap or the lead-lag angle. Consequently, the flap angle measurement was obtained by inferring the blade slope at $0.32 r/R$ from the bending moment at $0.048 r/R$. This slope was defined to be the flap angle. The lead/lag angle was measured, using a linear potentiometer located near the root of the blade."

4. TEST RESULTS

In order to validate the control system approach, test data from open-loop excitation of the Model 412 rotor were used to verify proper operation of the various components within the control loop. These steps consisted of validating the signal processing required to generate lag position and lag rate estimates, identifying the rotor transfer functions from swash plate inputs to lag accelerometer outputs, and analyzing the disturbance rejection capability and stability of the overall closed-loop system. Test data from the rotor were recorded in two formats, as 54 channels of digitized data sampled at 128 points per revolution for 15 revolutions, and as selected analog signals on a 14-channel FM tape recorder. The digitized data were converted to engineering units prior to storage, while the analog channels provided continuous signals for discrimination of low frequency signal amplitude and phase characteristics.

Both data sets exhibited poor signal-to-noise characteristics for the lag position sensor, except for initial rotor spin-up transients recorded on the analog tape. These transient signals were used to verify the operation of the observer in extracting both lag displacement and lag rate signals from the two lag accelerometers mounted on each blade. Since direct rotor rpm was not available in these transient data, rotor azimuth was inferred from time differences of $1/rev$ pulses on a separate channel. These smoothed rpm estimates were used in a modified form of the lag position and rate observer/filter that allowed variable integration steps as a function of rpm. Thus, proper treatment was made for the variable centrifugal acceleration components in the lag accelerometers during the spin-up process. Allowances were not made, however, for the direct component of sensor content due to shaft angular acceleration, since this would mean differentiation of an approximated rpm estimate. Despite this discrepancy, comparison of the lag sensor and the reconstructed lag signal from the observer in Figure 5 shows surprisingly good agreement, verifying the approach for generation of rotor states from blade mounted accelerometers.

The analog data was then used to find the spectral response characteristics of the Model 412 rotor to swash plate oscillations at discrete frequencies. Data records from 10 to 40 seconds were collected from the 8 accelerometers at each fixed excitation frequency to eliminate transient contamination of the spectral estimates. Two flight conditions were investigated, corresponding to an approximate hover condition and an advance ratio of 0.1. Example hover condition transfer functions from blade pitch to both inboard and outboard lag accelerometers on one of the blades are shown in Figure 6 and 7. The close match of both the magnitude and the slope of the phase curve around the lag resonance frequency (approximately $0.65/rev$) suggests that the simplified mathematical model used to produce the theoretical response curves should be adequate for lag damping augmentation design. The zeros in the magnitude response due to the accelerometers are not well defined by the response data, as they are at frequencies of $1.55/rev$ and $1.95/rev$ for the inboard and outboard sensors, respectively, above the excitation frequencies present in the test.

The final control system evaluation step concerned the investigation of the disturbance rejection capability of the control system design. This was achieved through comparison of the rotor pitch excitation used in the open-loop testing with the calculated rotor pitch to be fed back from the controller. Should these two signals cancel, one may infer that any other disturbances that would cause lag excitation could also be reduced through control of blade pitch through the swash plate. Figure 8 compares the pitch excitation measured on one of the blades with the pitch feedback signal from the controller. This feedback trace is inverted and offset in order to more closely compare the two signals. The controller output is the recombination of the feedback swash plate inputs in the rotating frame reference. The two curves can be seen to have similar shape, with the feedback signal slightly delayed due to the phase lag inherent in the filtering process.

The transfer function from the measured blade pitch to that generated by the control system was also computed using the open-loop frequency response data. Since the rotor was excited at discrete frequencies, each transfer function from the measured blade pitch to the 8 accelerometers was properly phase and magnitude shifted, and then combined to produce an equivalent feedback pitch signal. Since the output from the controller is for specific swash plate inputs, pure IBC feedback is not possible. From Figure 2, it can be shown that the resulting pitch feedback signal for blade "A" of the four-bladed rotor is:

$$\theta_{feedback} = K_R (3 \zeta_a + \zeta_b - \zeta_c + \zeta_d) / 4$$

after the collective and cyclic feedbacks are re-modulated through the swash plate into the rotating frame. True IBC feedback of ζ_a only would also require differential collective control. Note however that for the special case $\omega_L = \Omega$, e.g., ground resonance, IBC is achieved.

The resulting frequency response from measured pitch to controller output (with the pitch feedback inverted) is shown for the data at advance ratio of 0.1 in Figure 9. A theoretical response curve computed from the equivalent operations performed on the simplified linear model is also presented, and shows excellent correlation with the reconstructed test data feedback response.

5. CONCLUSIONS

1. The successful use of blade-mounted accelerometers to measure helicopter rotor blade lag response is experimentally verified.
2. The successful use of blade-mounted accelerometers as sensors in the feedback control of helicopter rotor blade lag response is experimentally verified.

Acknowledgements.

The authors greatly appreciate the assistance of Sam Greenhalgh of the Naval Air Development Center in the reproduction of the analog test data, and of Ruth Heffernan, Muhammed Hoque, Steve Jacklin, Alex Louie, and Tom Norman of Ames Research Center, NASA, in the acquisition of the test data.

REFERENCES

1. Ham, N. D., "Helicopter Individual-Blade-Control Research at MIT 1977-1985," *Vertica*, 11, 1/2, 1987.
2. Ham, N. D.; Balough, D.L.; and Talbot, P.D., "The Measurement and Control of Helicopter Blade Modal Response Using Blade-Mounted Accelerometers", *Proc. Thirteenth European Rotorcraft Forum*, September, 1987.
3. Ham, N. D., "Helicopter Gust Alleviation, Attitude Stabilization, and Vibration Alleviation Using Individual-Blade Control Through A Conventional Swash Plate," *Proc. Forty-First Annual AHS Forum*, May, 1985.
4. Kaufman, L., and Peress, K., "A Review of Methods for Predicting Helicopter Longitudinal Response," *Journal of The Aeronautical Sciences*, March, 1956.
5. Myers, A.W., et al. "The Model 412 Multi-bladed Rotor System," *Proc. AHS National Specialists' Meeting on Rotor System Design*, Philadelphia, PA October, 1980.

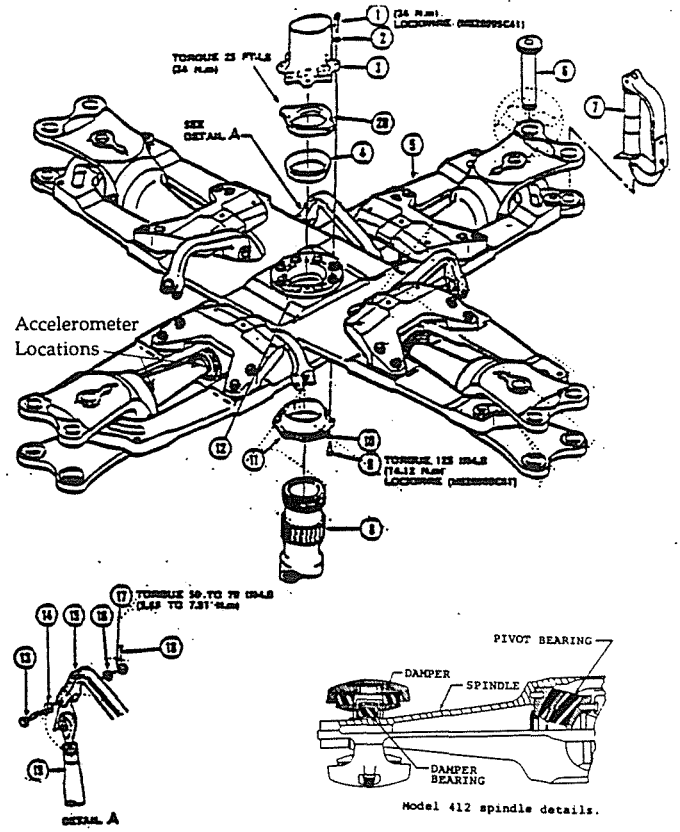


Figure 1. Model 412 Main Rotor Hub

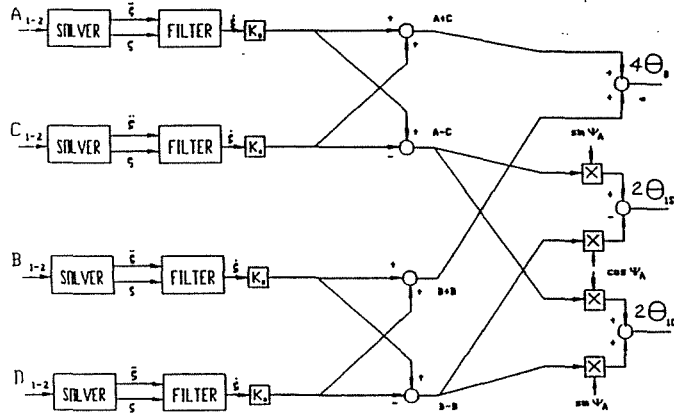


Figure 2. Schematic of Blade Lag Control System Using the Conventional Swash Plate: Four-Bladed Rotor.

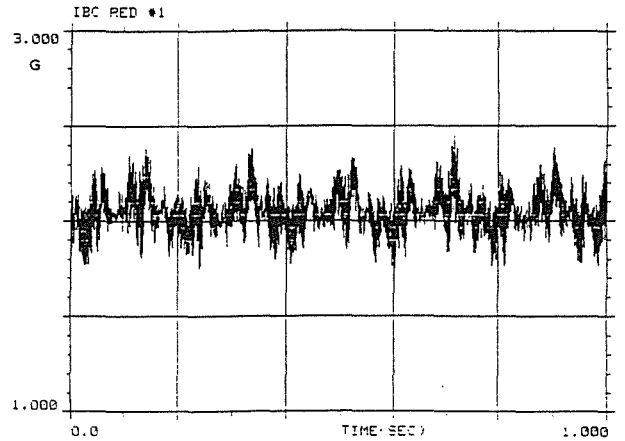


Figure 3. Typical lag Accelerometer Time History; $\mu = 0.1, \omega = 1.8 \text{ Hz}$.

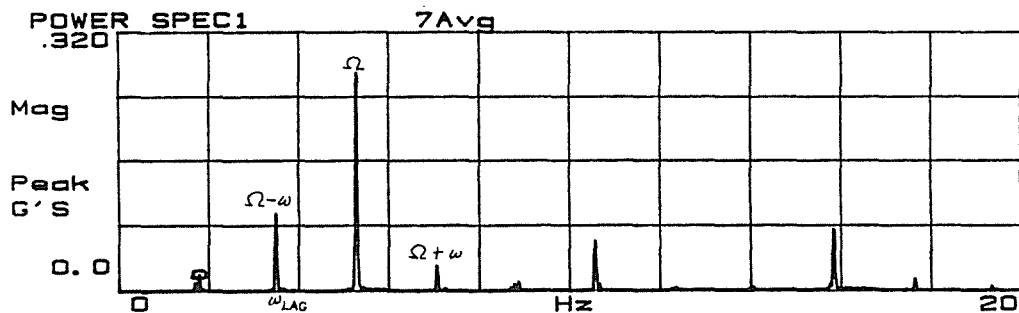


Figure 4. Typical Lag Accelerometer Frequency Spectrum; $\mu = 0.2, \omega = 1.8 \text{ Hz}$.

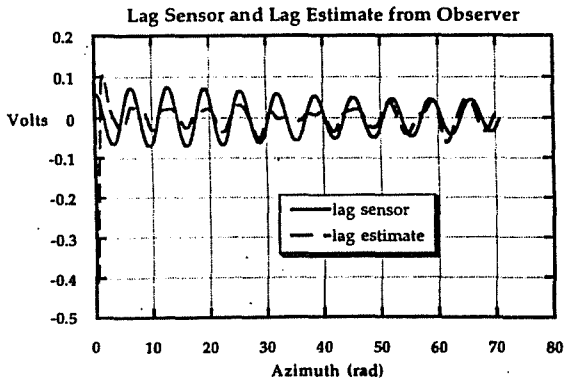


Figure 5. Comparison of Blade Lag Angle as Measured by Potentiometer and by Accelerometers.

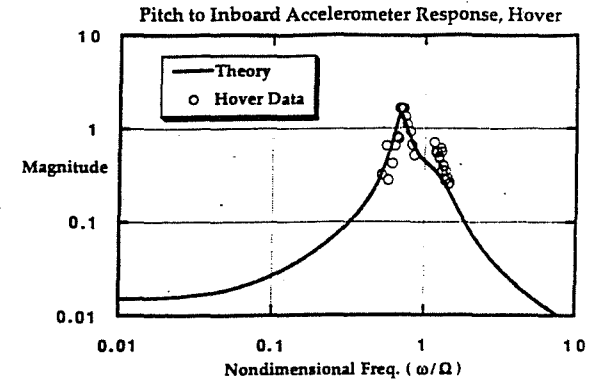
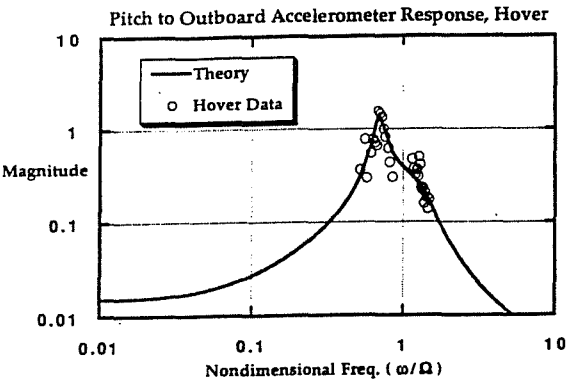


Figure 6. Blade Lag Normalized Accelerometer Response versus Pitch Excitation Frequency - Inboard Accelerometer

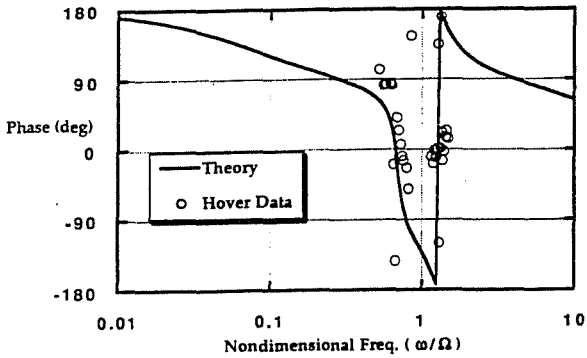


Figure 7. Blade Lag Normalized Accelerometer Response versus Pitch Excitation Frequency - Outboard Accelerometer

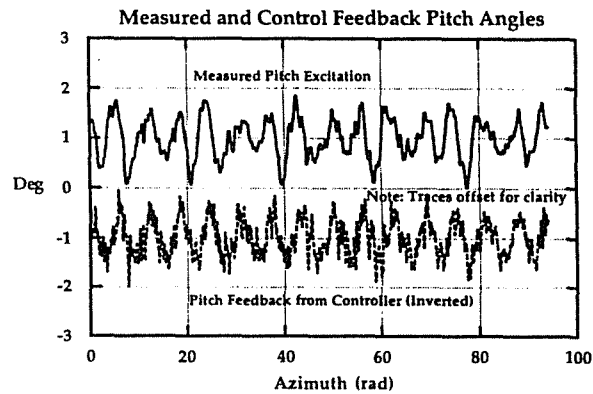


Figure 8. Comparison of Blade Pitch Excitation and IBC Pitch Feedback (Open Loop): Hover

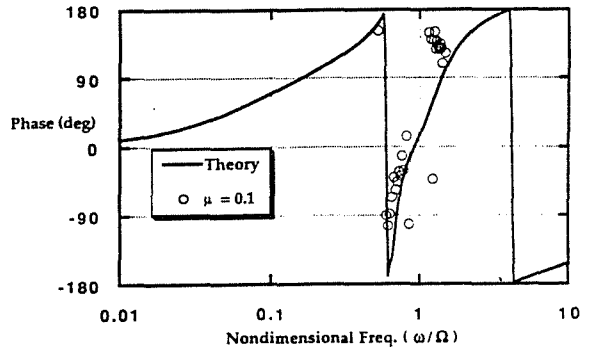
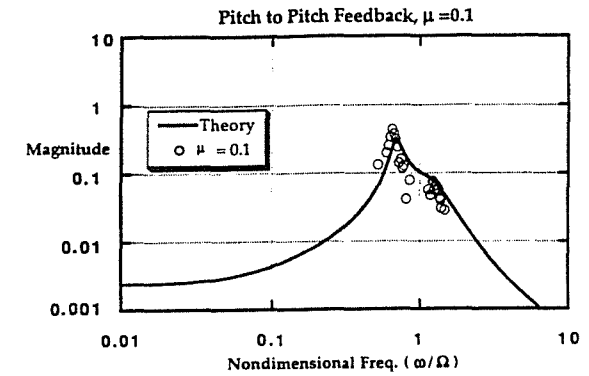


Figure 9. Open Loop Transfer Function from Blade Pitch Excitation to IBC Pitch Feedback versus Pitch Excitation Frequency

APPENDIX TO
RESEARCH ON MEASUREMENT AND CONTROL OF HELICOPTER ROTOR
RESPONSE USING BLADE-MOUNTED ACCELEROMETERS 1990-91

Norman D. Ham
M.I.T.

ABSTRACT

Recent developments in IBC technology and related rotor state measurements are briefly described.

It is shown that the concept of an imaginary swash plate applied to IBC systems leads to useful filtering of the blade-mounted accelerometer signals, while permitting the control of a four-bladed rotor using measurements from any three blades (if necessary).

Rotor state measurements in the rotating system are transformed to the corresponding non-rotating rotor states using the IBC algorithm, with its associated filtering properties, and measurements from any three blades (if necessary).

The application of narrow-band disturbance rejection techniques to IBC systems is briefly discussed.

1. INTRODUCTION

The concept of Individual-Blade-Control (IBC) embodies the control of broadband electrohydraulic actuators attached to each blade, using signals from sensors mounted on the blades to supply appropriate control commands to the actuators. Note that IBC involves not only control of each blade independently, but also a feedback loop for each blade in the rotating frame. In this manner it becomes possible to reduce the severe effects of atmospheric turbulence, retreating blade stall, blade-vortex interaction, blade-fuselage interference, and blade and rotor instabilities, while providing improved performance and flying qualities [1-10].

It is evident that the IBC system will be most effective if it is comprised of several sub-systems, each controlling a specific mode, e.g., the blade flapping mode, the first blade flatwise bending mode, and the first blade lag mode [2]. Each sub-system operates in its appropriate frequency band.

Consider the modal equation of motion

$$m\ddot{x} + c\dot{x} + kx = P(t) + \Delta F \quad (1)$$

where the modal control force ΔF is

$$\Delta F = -K_A m\ddot{x} - K_R c\dot{x} - K_P kx \quad (2)$$

Then substituting (2) into (1)

$$(1+K_A)m\ddot{x} + (1+K_R)c\dot{x} + (1+K_P)kx = P(t)$$

For the case $K_A = K_R = K_P = K$

$$m\ddot{x} + c\dot{x} + kx = [1/(1+K)] P(t)$$

and the modal response is attenuated by the factor $1/(1+K)$ while the modal damping and natural frequency are unchanged.

For modal damping augmentation, only the rate feedback $\Delta F = -K_R c\dot{x}$ is required.

The configuration considered in [1-7] employs an individual actuator and multiple feedback loops to control each blade. These actuators and feedback loops rotate with the blades and, therefore, a conventional swash plate is not required. However, some applications of individual-blade-control can be achieved by placing the actuators in the non-rotating system and controlling the blades through a conventional swash plate as described in Section 6 and in [8].

This research was sponsored by the Ames Research Center, NASA, under Cooperative Agreements NCC-2-366 and NCC-2-447.

2. DETERMINATION OF BLADE MODAL RESPONSE

The following sections describe the design of a system controlling blade flapping, bending, and lag dynamics, and related testing of the system on a model rotor in the wind tunnel. The control inputs considered are blade pitch changes proportional to blade flapping and bending acceleration, velocity, and displacement, and lag velocity. It is then shown that helicopter gust alleviation/attitude stabilization, vibration alleviation, and 1P lag damping augmentation can be achieved using the conventional helicopter swash plate for an N-bladed rotor where $N \geq 3$. For $N \geq 3$, all applications can be achieved.

From Figures 1 and [5], the blade flatwise acceleration at station r due to response of the first two flatwise modes is

$$a(r) = (r-e)\ddot{\beta}(t) + r\dot{\beta}^2(t) + \eta(r)\ddot{g}(t) + r\dot{g}^2(t)\eta'(r)$$

Then, for accelerometers mounted at $r_1, r_2, r_3,$ and r_4

$$\begin{bmatrix} a_1 \\ a_2 \\ a_3 \\ a_4 \end{bmatrix} = \begin{bmatrix} (r_1-e) & r_1\dot{\beta}^2 & \eta(r_1) & r_1\dot{g}^2\eta'(r_1) \\ (r_2-e) & r_2\dot{\beta}^2 & \eta(r_2) & r_2\dot{g}^2\eta'(r_2) \\ (r_3-e) & r_3\dot{\beta}^2 & \eta(r_3) & r_3\dot{g}^2\eta'(r_3) \\ (r_4-e) & r_4\dot{\beta}^2 & \eta(r_4) & r_4\dot{g}^2\eta'(r_4) \end{bmatrix} \begin{bmatrix} \ddot{\beta} \\ \dot{\beta} \\ \ddot{g} \\ \dot{g} \end{bmatrix}$$

In matrix notation, $A = M \cdot R$

Then the flatwise modal responses are given by

$$R = M^{-1} \cdot A$$

Note that the elements of M^{-1} are dependent only upon blade spanwise station, rotor rotation speed, and bending mode shape, i.e., they are independent of flight condition.

Similarly, the blade lag acceleration at station r due to response of the first lag mode can be shown to be [6]

$$a_L = (r - e_L)\ddot{\zeta} + e_L\dot{\zeta}^2$$

where e_L is the spanwise location of the lag hinge. Then for accelerometers mounted at r_1 and r_2

$$\begin{bmatrix} a_{L1} \\ a_{L2} \end{bmatrix} = \begin{bmatrix} (r_1 - e_L) & e_L\dot{\zeta}^2 \\ (r_2 - e_L) & e_L\dot{\zeta}^2 \end{bmatrix} \begin{bmatrix} \ddot{\zeta} \\ \dot{\zeta} \end{bmatrix}$$

In matrix notation $A_L = M_L \cdot R_L$

The lag modal responses are given by

$$R_L = M_L^{-1} \cdot A_L$$

Since the elements of M^{-1} and M_L^{-1} are independent of flight condition, the solution for a desired modal response involves only the summation of the products of spanwise accelerometer signals and their corresponding constant matrix elements by an analog or digital device, here called a solver.

3. IDENTIFICATION OF MODAL RATE RESPONSE

Consider the block diagram shown in Figure 2. For modal acceleration \ddot{x} and modal displacement x determined as above for any mode, this diagram represents the following filter equations from [7,9]:

$$\frac{d}{dt} \hat{x} = \hat{x} + K_1(x - \hat{x}) \quad (3)$$

$$\frac{d}{dt} \dot{\hat{x}} = \dot{\hat{x}} + K_2(x - \hat{x}) \quad (4)$$

where the hatted quantities are estimated values, and K_1 and K_2 are constants. Writing the estimation error as

$$e = x - \hat{x}$$

and differentiating equation (3) with respect to time, there results

$$\frac{d^2}{dt^2} \hat{x} = \frac{d}{dt} \dot{\hat{x}} + K_1 \dot{e} \quad (5)$$

Substituting equation (4) into equation (5),

$$\frac{d^2}{dt^2} \hat{x} = \ddot{x} + K_2 e + K_1 \dot{e} \quad (6)$$

Since $\frac{d^2}{dt^2} \hat{x} - \ddot{x} = -\ddot{e}$, equation (6) becomes

$$\ddot{e} + K_1 \dot{e} + K_2 e = 0 \quad (7)$$

This expression represents the dynamics of the estimation error. The corresponding characteristic equation is

$$s^2 + K_1 s + K_2 = 0$$

The bandwidth and damping of the estimation process are determined by the choice of the constants K_1 and K_2 .

Since the elements of the filter shown in Figure 2 are independent of flight condition, the estimation of modal rate response involves only the integration of the products of constants and the measured modal responses by an analog or digital device, here called a McKillip filter. Note that an improved estimate of the modal displacement x is also obtained due to the double integration of modal acceleration \ddot{x} embodied in the filter. Also, note that no knowledge of the rotor or its flight condition is required in designing the filter.

4. FORM OF THE MODAL CONTROLLER

As discussed in the Introduction, the modal controller voltage output to the blade pitch actuator is proportional to modal acceleration, rate, and displacement:

$$V = -K_A \ddot{x} - K_R \dot{x} - K_P x$$

where K_A , K_R , and K_P are constants and therefore independent of flight condition.

For modal damping augmentation only,

$$V = -K_R \dot{x}$$

5. MODAL CONTROL BY INDIVIDUAL- BLADE- CONTROL (IBC)

The solver, McKillip filter, and controller described in Sections 2-4 are combined to form the IBC system for a given mode. The combined functions of the solver and the McKillip filter are here called the "observer". Some applications are described below, including experimental results obtained at MIT from a four-foot-diameter wind tunnel model rotor, using IBC.

Reference [3] describes the application of IBC to helicopter gust alleviation. The feedback blade pitch control was proportional to blade flapping acceleration and displacement, i.e.,

$$\Delta\theta = -K \left(\frac{\ddot{\beta}}{\omega^2} + \beta \right)$$

A block diagram of the control system is shown in Figure 3. Note that each blade requires only two flatwise-oriented blade-mounted accelerometers.

Figure 4 shows the effect of increasing the open-loop gain K upon the IBC gust alleviation system performance. Note that the experimental reduction in gust-induced flapping response is in accordance with the theoretical closed-loop gain $1/(1+K)$.

The Lock number of the model blade was 3.0. For a full size rotor, the increase in damping due to the increase in Lock number results in the flapping at excitation frequency becoming the dominant response. Also, with increased blade damping it becomes possible to use higher feedback gain for the same stability level, and as a consequence the IBC system performance improves with increasing Lock number.

Following the successful alleviation of gust disturbances using the IBC system, Reference [3] showed the theoretical equivalence of blade flapping response due to atmospheric turbulence and that due to other low-frequency disturbances, e.g., helicopter pitch and roll attitude; therefore these disturbances can also be alleviated by the IBC system, as shown in [8], to provide helicopter attitude stabilization.

References [5,8] describe the application of IBC to rotor vibration alleviation. The feedback blade pitch control was proportional to blade bending acceleration, rate and displacement, i.e.,

$$\Delta\theta = -K_A \ddot{g} - K_R \dot{g} - K_P g$$

A block diagram of the system is shown in Figure 5. Note that each blade requires four flatwise-oriented blade-mounted accelerometers.

Preliminary experimental results presented in Figure 6 show the effect of increasing the IBC open-loop gain K from 0 to 3 upon the flatwise bending mode response. Note that the experimental reduction in vibratory bending response is in accordance with the theoretical closed-loop gain $1/(1+K)$.

Since a major source of helicopter higher harmonic vertical vibration is the blade flatwise bending response to the impulsive loading due to blade-vortex or blade-fuselage interaction, if the blade flatwise bending response is controlled, the higher harmonic vertical vibration will be correspondingly reduced, as shown in Figure 7, from [11].

It should be noted that suppression of blade flapping and flatwise bending responses and their corresponding in-plane Coriolis forces will tend to alleviate in-plane vibration as a beneficial by-product of vertical vibration alleviation.

Reference [6] describes the application of IBC to rotor lag damping augmentation. The feedback voltage to the blade pitch control actuator was proportional to blade lag rate, i.e.,

$$\tau \dot{V} + V = -K_R \dot{\gamma}$$

where the time delay is required for closed-loop stability. A block diagram of the system is shown in Figure 8. Note that each blade requires two lagwise-oriented blade-mounted accelerometers.

Figure 9 shows the effect of increasing the IBC open-loop gain on experimental blade lag damping. The figure shows a rotation of the slope of the phase angle versus frequency curve at lag resonance, in the direction of increased lag damping, as K_R is increased. The increase in lag damping ratio due to the control system was determined to be 0.37.

6. MODAL CONTROL USING A CONVENTIONAL SWASH PLATE

The preceding sections have demonstrated that the use of blade-mounted accelerometers as sensors makes possible the control of the flapping, flatwise bending, and lag modes of each blade individually. This control technique is applicable to helicopter rotor gust alleviation, attitude stabilization, vibration alleviation, and lag damping augmentation.

For rotors having three blades, any arbitrary pitch time history can be applied to each blade individually using the conventional swash plate. Rotors with more than three blades require individual actuators for each blade for some applications; other applications such as gust alleviation, attitude stabilization, vibration alleviation, and 1P lag damping augmentation can be achieved using a conventional swash plate, as shown below and in [8].

If the control requirement for the m th blade of an N -bladed rotor is θ_m , determined using blade-mounted accelerometers as described in Section 2, then the corresponding control requirement for the swash plate is

$$\theta = \theta_0 + \theta_{1c} \cos \psi + \theta_{1s} \sin \psi + \theta_2$$

Using the mathematics of [12], P. 351, the control laws are

$$\theta_0 = \frac{1}{N} \sum_{m=1}^N \theta_m = 0 \text{ unless } n = pN$$

$$\theta_{1c} = \frac{2}{N} \sum_{m=1}^N \theta_m \cos \psi_m = 0 \text{ unless } n = pN \pm 1$$

$$\theta_{1s} = \frac{2}{N} \sum_{m=1}^N \theta_m \sin \psi_m = 0 \text{ unless } n = pN \pm 1$$

$$\theta_2 = 0 \text{ unless } n = pN \pm N/2 \text{ [12], P. 348}$$

where p = any integer
 n = rotor harmonic number

The physical significance of the above equations is that IBC of an N -bladed rotor having a conventional swash plate is possible for those IBC functions involving the zeroth (quasi-steady), first, N th, and $(N \pm 1)$ th harmonics of rotor speed, e.g., gust alleviation ($p=0$), attitude stabilization ($p=0$), vibration alleviation ($p=1$), and 1P lag damping augmentation ($p=0$).

Note that all harmonics and in general any arbitrary time history of control are achievable with a three-bladed rotor using a conventional swash plate.

The summations of individual blade sensor signals required to obtain the swash plate collective and cyclic pitch components provide a filtering action such that only the desired harmonics 0P, 1P, NP, and $(N \pm 1)P$ remain after summation, i.e., no specific harmonic analysis is required.

Since all sensing is done in the blades, no transfer matrices from non-rotating to rotating system are required; therefore no updating of these matrices is required, and no non-linearity problems result from the linearization required to obtain the transfer matrices. Also, blade state measurements allow tighter vehicle control since rotor control can lead fuselage response: this lead should provide more effective gust alleviation and permit higher control authority without inducing rotor instabilities than would be possible without rotor state feedback [13].

A block diagram of an active control system for the conventional swash plate of a helicopter rotor having four blades A, B, C, and D is shown in Figure 10. The control voltages V_{A-D} are generated from blade-mounted accelerometer signals, as described in preceding sections. A schematic showing all the components of such an active control system is shown in Figure 11 for the special case of vibration alleviation.

7. CONTROL OF FOUR-BLADED ROTORS USING MEASUREMENTS FROM THREE BLADES

Following Section 6, the control requirements for a four-bladed rotor in terms of individual blade control requirements $\theta_1, \theta_2, \theta_3$, and θ_4 are given by:

$$\theta_0 = 1/4 (\theta_1 + \theta_2 + \theta_3 + \theta_4) \quad n = 0, 4, 8, \dots \quad (8)$$

$$\theta_{1c} = 1/2 (\theta_1 \cos \psi_1 + \theta_2 \sin \psi_1 - \theta_3 \cos \psi_1 - \theta_4 \sin \psi_1) \quad n = 1, 3, 5, \dots \quad (9)$$

$$\theta_{1s} = 1/2 (\theta_1 \sin \psi_1 - \theta_2 \cos \psi_1 - \theta_3 \sin \psi_1 + \theta_4 \cos \psi_1) \quad n = 1, 3, 5, \dots \quad (10)$$

$$\theta_D = 1/4 (\theta_1 - \theta_2 + \theta_3 - \theta_4) \quad n = 2, 6, 10, \dots \quad (11)$$

where the first three quantities are the conventional swash plate control degrees of freedom, and θ_D is a differential collective control not available from a conventional swash plate. In the present case, an imaginary swash plate is postulated, even though individual-blade-control is used.

Note the filtering action implied by equations 8 - 11. The summation process acts as a narrow-band filter passing only the 0P, 4P, etc. harmonics (θ_0), the 1P, 3P, etc., harmonics (θ_{1c} and θ_{1s}), or the 2P, 6P, etc. harmonics (θ_D).

If only θ_1, θ_2 , and θ_3 are available due to failure or other constraints, θ_4 can be eliminated from equations 8 - 11 to yield the following relationships:

$$\theta_0 + \theta_D = 1/2 (\theta_1 + \theta_3)$$

$$\theta_{1c} = 1/2 [\theta_1 \cos \psi_1 + \theta_2 \sin \psi_1 - \theta_3 \cos \psi_1 - (\theta_1 - \theta_2 + \theta_3) \sin \psi_1]$$

$$\theta_{1s} = 1/2 [\theta_1 \sin \psi_1 - \theta_2 \cos \psi_1 - \theta_3 \sin \psi_1 + (\theta_1 - \theta_2 + \theta_3) \cos \psi_1]$$

Then for the m th IBC blade in general,

$$\theta_m = \theta_0 + \theta_{1c} \cos \psi_m + \theta_{1s} \sin \psi + \theta_D$$

In the failure case $\theta_D = 0$. This means that control of the differential collective mode of blade flapping and/or bending is not available. This consequence would only be significant if control of the second and/or sixth flapping and/or bending harmonics were required: this is not the case for control of blade flapping and/or bending of a four-bladed rotor, which requires the control of the zeroth, first, third, fourth, and fifth harmonics only.

8. MEASUREMENT OF FOUR-BLADED ROTOR STATES

Following Section 6, the non-rotating flapping coordinates for a four-bladed rotor in terms of individual blade control requirements $\beta_1, \beta_2, \beta_3$, and β_4 are given by the equations:

$$\beta_0 = 1/4 (\beta_1 + \beta_2 + \beta_3 + \beta_4) \quad n = 0, 4, 8, \dots \quad (12)$$

$$\beta_{1c} = 1/2 (\beta_1 \cos \psi_1 + \beta_2 \sin \psi_1 - \beta_3 \cos \psi_1 - \beta_4 \sin \psi_1) \quad n = 1, 3, 5, \dots \quad (13)$$

$$\beta_{1s} = 1/2 (\beta_1 \sin \psi_1 - \beta_2 \cos \psi_1 - \beta_3 \sin \psi_1 + \beta_4 \cos \psi_1) \quad n = 1, 3, 5, \dots \quad (14)$$

$$\beta_D = 1/4 (\beta_1 - \beta_2 + \beta_3 - \beta_4) \quad n = 2, 6, 10, \dots \quad (15)$$

shown in schematic form in Figure 12. The β_D branch is omitted for clarity.

Note the filtering action implied by equations 12-15. The summation process acts as a narrow-band filter passing only the 0P, 4P, etc. harmonics (β_0), the 1P, 3P, etc., harmonics (β_{1c} and β_{1s}), or the 2P, 6P, etc. harmonics (β_D).

If only β_1, β_2 , and β_3 are available due to failure or other constraints, β_4 can be eliminated from equations 12-15 to yield the following relationships:

$$\beta_0 + \beta_D = 1/2 (\beta_1 + \beta_3) \quad (16)$$

$$\beta_{1c} = 1/2 [\beta_1 \cos \psi_1 + \beta_2 \sin \psi_1 - \beta_3 \cos \psi_1 - (\beta_1 - \beta_2 + \beta_3) \sin \psi_1] \quad (17)$$

$$\beta_{1s} = 1/2 [\beta_1 \sin \psi_1 - \beta_2 \cos \psi_1 - \beta_3 \sin \psi_1 + (\beta_1 - \beta_2 + \beta_3) \cos \psi_1] \quad (18)$$

Then for the mth IBC blade in general,

$$\beta_m = \beta_0 + \beta_{1c} \cos \psi_m + \beta_{1s} \sin \psi + \beta_D$$

where the reconstituted blade coordinate β_m retains the filtered characteristics of β_0 , β_{1c} , β_{1s} , and β_D .

The corresponding non-rotating flapping rates can be obtained by differentiating equations 12-15 with respect to time. The result is shown schematically in Figure 13. The failure case can be obtained by differentiating equations 16-18.

In the failure case β_D is indeterminate. This consequence would only be significant if control of the second and/or sixth flapping harmonics were required: this is not the case for attitude control and vibration alleviation of a four-bladed rotor, which requires the control of the zeroth, first, third, fourth, and fifth harmonics only.

9. NARROW-BAND CONTROL OF IBC ROTORS

Current IBC systems utilize broad-band control of disturbances, i.e., they are designed to operate over a wide range of frequencies. Consequently, they may be gain-limited in some cases by stability considerations. For some applications, e.g., vibration alleviation, it may be advantageous to use narrow-band disturbance rejection techniques.

Reference 14 contains an excellent analysis and summary of such techniques. It demonstrates that current HHC systems embody control elements of the form

$$H(s) = \frac{as + b}{s^2 + \omega_0^2} \quad (19)$$

in the feedback loop. Such an element is designed to reject a harmonic signal of frequency ω_0 , since it is infinite at $s = i\omega_0$, implying infinite feedback gain. The constants a and b are chosen to ensure closed loop system stability. Their magnitudes determine the disturbance rejection band width.

Reference 14 presents a typical HHC control system in Fig. 5 of that reference, reproduced here as Fig. 14, where T^{-1} is the inverse of the control response matrix of the plant, and $N\Omega$ is the frequency of the component of disturbance d to be rejected. The reference demonstrates that the system of Fig. 14 can be reduced to the form of equation 19 where in this case $\omega_0 = N\Omega$. The reference shows this system has the desired properties of stability robustness and disturbance rejection, even with no adaptation of the T matrix, as long as the initial choice of T is reasonably close to its actual value.

The vibration control system of Fig. 14 can be implemented in IBC form. In a typical case, the plant to be controlled is the blade flatwise bending mode near resonance with the third harmonic airload. Using the hovering form for simplicity, the bending transfer function is the simple second order plant:

$$\frac{g(s)}{\theta(s)} = \frac{C}{s^2 + 2\zeta\omega_n s + \omega_n^2} \quad (20)$$

Note that in the present simple case, this replaces the control matrix T. Then since the inverse of equation 20 appears in the feedback loop as $K_A s^2 + K_R s + K_P$ (Fig. 11), pole-zero cancellation is achieved between the control zeroes and the plant poles (equation 20). This contributes to the stability of the system, and offsets the destabilizing effect of the near conjunction of controller poles and the bending mode poles ($\omega_0 = \omega_n$) shown in Fig. 7 of Ref. 14.

Fig. 11 shows the current, broad-band form of an IBC blade-bending control system. The modification to a narrow-band system is shown in Fig. 15 for blade A. This modification would be applied to all blades shown in Fig. 11 in a similar manner.

10. CONCLUSIONS

1. The use of blade-mounted accelerometers to measure or estimate blade flapping, lagging, and bending accelerations, rates, and displacements is shown to be feasible.
2. The application of the concept of an imaginary swash plate to IBC systems leads to useful filtering of the blade accelerometer signals, while permitting the control of a four-bladed rotor using measurements from any three blades (if necessary).
3. Rotor state measurements in the rotating system can be transformed to the corresponding non-rotating rotor states using the IBC algorithm, with its associated filtering properties, and measurements from any three blades (if necessary).
4. Narrow-band disturbance rejection techniques can be readily applied to IBC systems. The pole-zero cancellations inherent in these systems greatly enhances the robustness of the overall system.

REFERENCES

1. Kretz, M., "Research in Multicyclic and Active Control of Rotary Wings," *Vertica* 1, 95-105, 1976.
2. Ham, N.D., "A Simple System for Helicopter Individual-Blade-Control Using Modal Decomposition", *Vertica*, 4, 23-28, 1980.
3. Ham, N.D. and McKillip, R.M., Jr., "A Simple System for Helicopter Individual-Blade-Control and Its Application to Gust Alleviation", *Proc. Thirty-Sixth AHS Annual National Forum*, Washington, D.C., May 1980.
4. Ham, N.D. and Quackenbush, T.R., "A Simple System for Helicopter Individual-Blade-Control and Its Application to Stall-Induced Vibration Alleviation", *Proc. AHS National Specialists' Meeting on Helicopter Vibration*, Hartford, CT, November 1981.
5. Ham, N.D., "Helicopter Individual-Blade-Control and Its Applications", *Proc. Thirty-Ninth AHS Annual National Forum*, St. Louis, MO, May 1983.
6. Ham, N.D., Behal, Brigitte L. and McKillip, R.M., Jr., "Helicopter Rotor Lag Damping Augmentation Through Individual-Blade-Control", *Vertica*, 7, 361-371, 1983.
7. McKillip, R.M. Jr., "Periodic Control of the Individual-Blade-Control Helicopter Rotor", *Vertica*, 9, 199-224, 1985.
8. Ham, N.D., "Helicopter Gust Alleviation, Attitude Stabilization, and Vibration Alleviation Using Individual-Blade-Control Through a Conventional Swash Plate", *Proc. Forty-First AHS Annual National Forum*, Fort Worth, Texas, May 1985.
9. McKillip, R.M. Jr., "Kinematic Observers for Rotor Vibration Control", *Proc. Forty-Second AHS Annual National Forum*, June 1986.
10. Ham, N.D., "Helicopter Individual-Blade-Control Research at MIT 1977-1985," *Vertica* 11, 109-122, 1987.
11. Leone, P.F., "A Method for Reducing Helicopter Vibration," *JAFS* 2, 3, July 1957.
12. Johnson, W., *Helicopter Theory*, Princeton U.P., 1980.
13. DuVal, R.W., "Use of Multiblade Sensors for On-Line Rotor Tip-Path-Plane Estimation," *JAFS* 25, 4, October 1980.
14. Hall, S. R. and Wereley, N. M., "Linear Control Issues in the Higher Harmonic Control of Helicopter Vibrations", *Proceedings of the 45th Annual Forum of the AHS*, Boston, MA, May 1989.

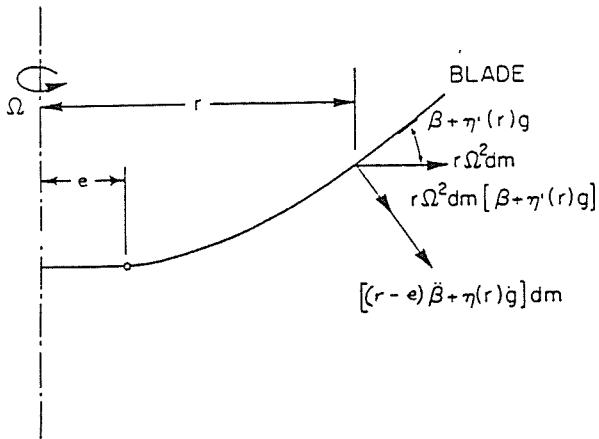


Figure 1. Blade Flatwise Inertia Forces

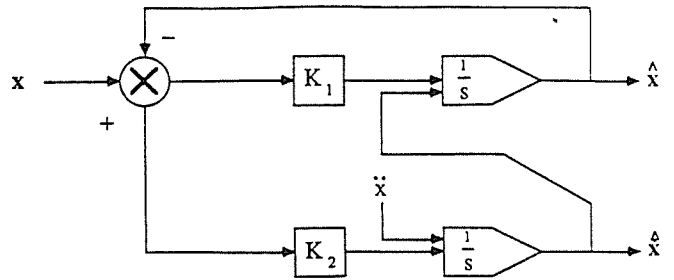


Figure 2. Block Diagram of McKillip Filter

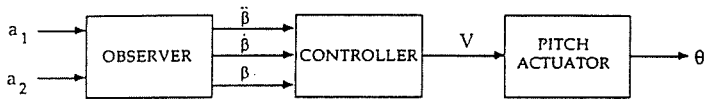


Figure 3. Block Diagram of Flapping IBC System

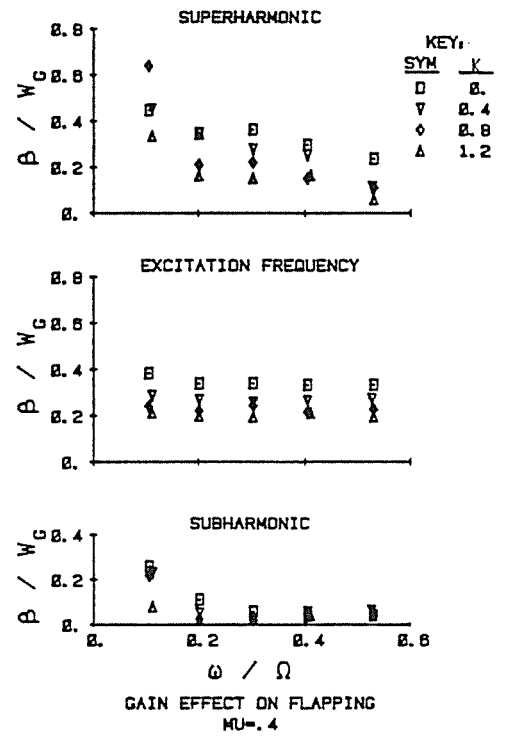


Figure 4. Effect of Feedback Gain on Flapping Response to Gust ($\mu = 0.4$)

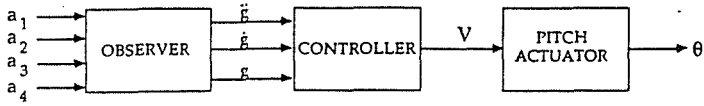


Figure 5. Block Diagram of Bending IBC System

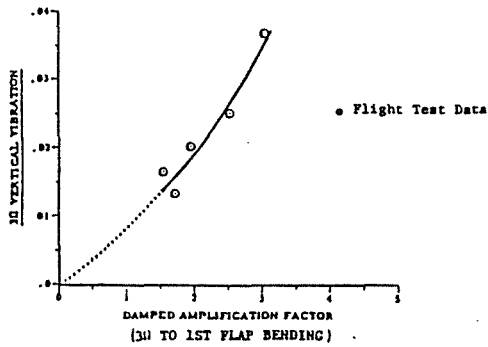


Figure 7. Effect of Blade Bending Amplification Factor on Maximum Cockpit Vibration Level

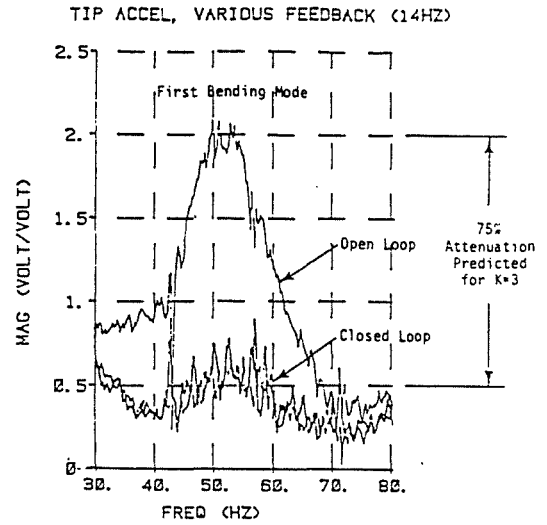


Figure 6. Open and Closed Loop Flatwise Tip Accelerometer Response to White Noise Pitch Input in Hover

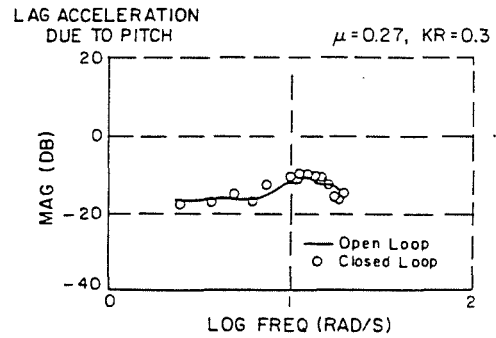


Figure 9. Open and Closed Loop Acceleration Response to White Noise Pitch Input ($\mu = 0.27$)

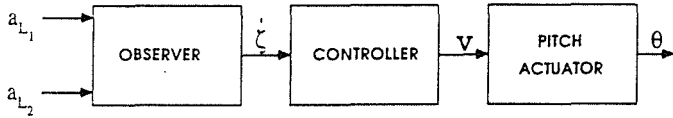
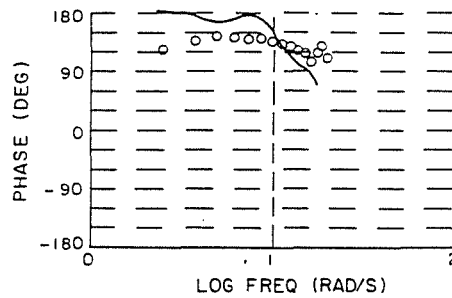


Figure 8. Block Diagram of Lag IBC System

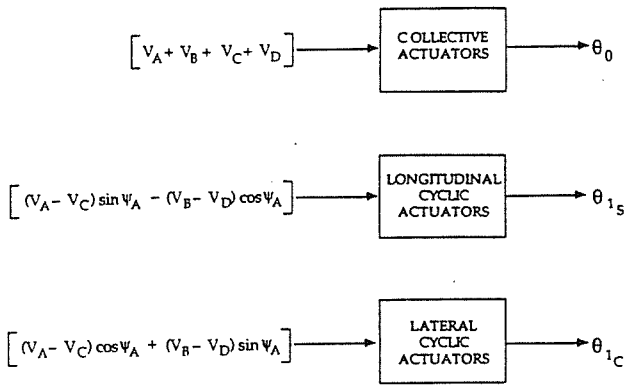


Figure 10. Block Diagram of Flapping, Bending, or Lag Control System Using the Conventional Swash Plate: Four-Bladed Rotor

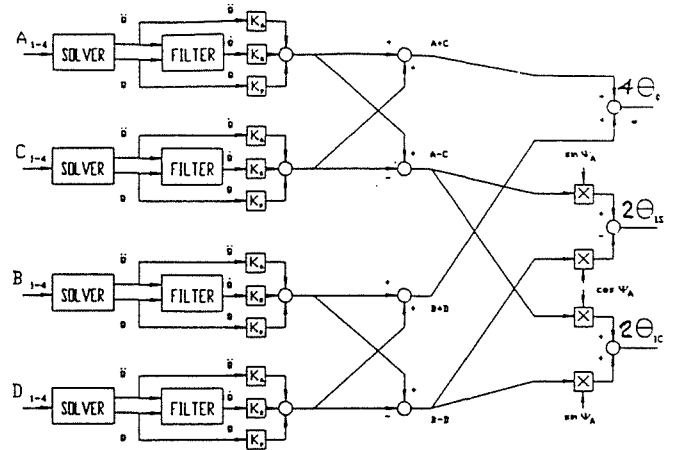


Figure 11. Schematic of Bending Control System Using the Conventional Swash Plate: Four-Bladed Rotor (Drawn by R.H. McKillip Jr.)

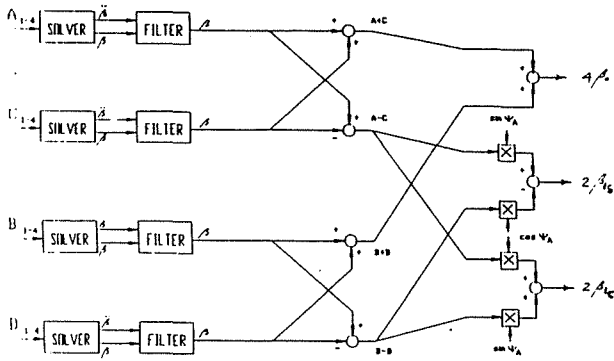


Figure 12. Schematic of Flapping Displacement Measurement System

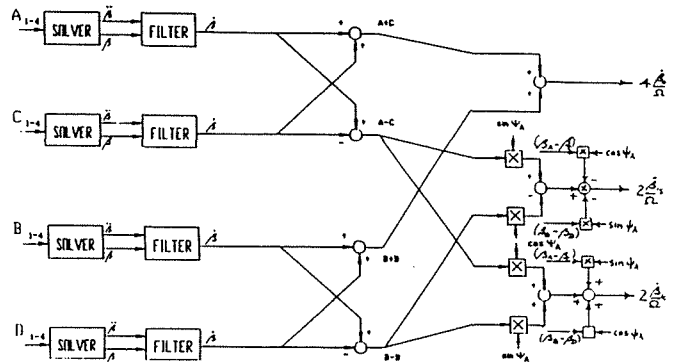


Figure 13. Schematic of Flapping Rate Measurement System

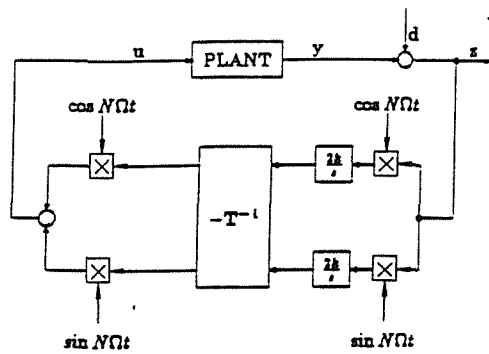


Figure 14. Implementation of higher harmonic control system in continuous time.

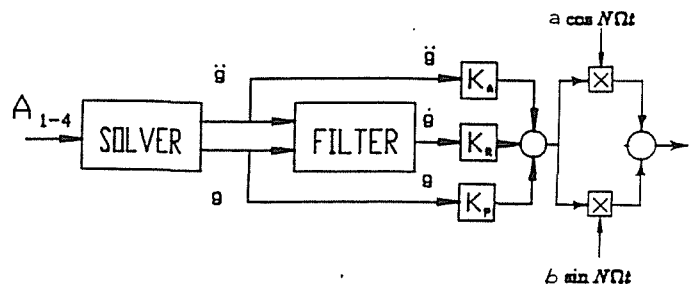


Figure 15. Narrow-Band IBC System